Dalton Transactions

Analysis of the isomer ratios of polymethylated-DOTA complexes and the implications on protein structural studies

Journal:	*Dalton Transactions*
Manuscript ID	DT-ART-08-2015-003210.R2
Article Type:	Paper
Date Submitted by the Author:	08-Jan-2016
Complete List of Authors:	Opina, Ana Christina; National Institutes of Health, Strickland, Madeleine; National Institutes of Health, Lee, Yong-Sok; National Institutes of Health, Tjandra, Nico; National Institutes of Health, Byrd, R. Andrew; National Institutes of Health, Swenson, Rolf; National Institutes of Health, Vasalatiy, Olga; National Institutes of Health,

Analysis of the isomer ratios of polymethylated-DOTA complexes and the implications on protein structural studies

Ana Christina L. Opina[*a], Madeleine Strickland[b], Yong-Sok Lee[c], Nico Tjandra[b], R. Andrew Byrd[d], Rolf E. Swenson[a], and Olga Vasalatiy[a]

[a] Imaging Probe Development Center, National Heart, Lung, and Blood Institute, National Institutes of Health, Rockville, MD 20850, United States

[b] Laboratory of Molecular Biophysics, National Heart, Lung, and Blood Institute, National Institutes of Health, Bethesda, MD 20892, United States

[c] Center for Molecular Modeling, Division of Computational Bioscience, Center for Information Technology, National Institutes of Health, Bethesda, MD 20892, United States

[d] Structural Biophysics Laboratory, National Cancer Institute, National Institutes of Health, Frederick, MD 21702, United States

ABSTRACT

A rigidified and symmetrical polymethylated 1,4,7,10-tetraazacyclododecane-1,4,7,10-tetraacetic acid (DOTA) ligand bearing four *SSSS* methyl groups in both the tetraaza ring and the acetate arms (*SSSS*-*SSSS*-M4DOTMA) was prepared. The isomer ratio of *SSSS*-*SSSS*-M4DOTMA complexed with a series of lanthanide ions was carefully investigated using RP-HPLC and NMR. A square antiprismatic (SAP) configuration was exclusively observed for the early lanthanides, while the twisted square antiprismatic (TSAP) geometry was preferred as the lanthanide ion size decreases. The late lanthanides adopted the TSAP geometry exclusively. One of the pendant arms was modified with a pyridyl disulfide group (*SSSS*-*SSSS*-M8SPy) for cysteine attachment and displayed a similar isomer trend as the parent compound, Ln-*SSSS*-*SSSS*-M4DOTMA. Covalent attachment to the ubiquitin S57C mutant showed resonances whose intensities are in agreement with the isomeric population observed by HPLC. Furthermore, the NOE experiments combined with quantum chemical calculations have unequivocally demonstrated that the SAP of Pr-*SSSS*-*SSSS*-M4DOTMA and Pr-*SSSS*-*SSSS*-M8SPy, as well as the TSAP of Yb-*SSSS*-*SSSS*-M8SPy are more stable than their corresponding isomers.

INTRODUCTION

Lanthanide metals have a rich history in providing contrast in magnetic resonance imaging (MRI), especially Gd^{3+} agents. They are administered in the form of a chelate to eliminate the toxicity of the Gd^{3+} ion. DOTA (1,4,7,10-tetraazacyclododecane-1,4,7,10-tetraacetic acid)-based ligands form some of the most thermodynamically stable and kinetically inert complexes with lanthanide ions [1-4]. This is due to a very good match between the size of the DOTA cavity and the lanthanide ions [5]. The lanthanide ion has 9 coordination sites, 8 of which are occupied by the macrocyclic ligand where the Ln^{3+} is sandwiched between two square planes of the four nitrogens from the macrocycle (N_4) and four oxygens from the pendant arm (O_4), while the remaining site is capped by a water molecule. It is well-known that lanthanide DOTA forms two isomers in solution – the monocapped Square Antiprism (SAP) and the monocapped Twisted Square Antiprism (TSAP) [6-9]. These isomers may interconvert, either by pendant arm rotation or by ring flipping motion (Fig. 1). The arm may rotate clockwise (Λ) or counterclockwise (Δ), and the ring may likewise display clockwise (λλλλ) or counterclockwise (δδδδ) helicities. This rotation results in two diastereomers, each being present as an enantiomeric pair: Δ(λλλλ), Λ(δδδδ) and Δ(δδδδ), Λ(λλλλ). The TSAP isomer is obtained for Δ(δδδδ) and Λ(λλλλ), which has the same helicities for both the tetraacetate arms and the tetraaza ring, while the opposite configuration is displayed by the SAP isomer, Δ(λλλλ) and Λ(δδδδ). The ratio of the TSAP and SAP isomers is governed by the size of the lanthanide ion, the ligand sidearms, and the shape of the ligand cavity.

Interest in these isomers lies in their different properties, based on different geometries. The TSAP isomer has a more "open" coordination cage with a smaller torsion angle between the O_4 and N_4 planes (~25^o), while the SAP isomer has a large torsion angle of ~39^o and a more compact structure [10]. The bound water molecule in the TSAP isomer lies further from the lanthanide ion, thus, water exchange has been shown to be 50 times faster in the TSAP isomer than in the SAP isomer [11-15].

Recently, a rigid macrocyclic ligand based on M4 cyclen, a tetra-methylated analogue of cyclen (Figure 2a) was synthesized and characterized by Ranganathan and co-workers [16]. This ligand, *SSSS*-*RRRR*-M4DOTMA (Fig. 2b), has four methyl substituents each on the tetraaza ring (*SSSS*)

and on the acetate arms (*RRRR*), and was found to form a highly rigid and symmetrical complex with Yb^{3+}. Since lanthanide ions can shift the magnetic resonance frequency of the nuclei in its vicinity (known as the lanthanide induced shift, LIS or pseudocontact shift, PCS), this rigidity is advantageous for extracting structural details of proteins in solution by conjugating the macromolecule to the lanthanide complex. Attachment of lanthanide DOTA derivatives to a protein has been reported in the past [17-21], however it suffers from two major drawbacks: first, is the fast motional averaging of the metal chelators relative to protein, resulting in significant reductions in the magnitude of PCS observed; second, is the presence of the SAP and TSAP isomers that cause additional resonances to be observed for each nucleus that experience the paramagnetic effect.

To this end, Haussinger and co-workers utilized Ranganathan's work by developing a modified M4DOTMA reagent, containing a pyridyl disulfide group modification to one of the arms, that permits conjugation with the free cysteines of a protein [22]. The rigid structure of the ligand, referred to as M8SPy (Fig. 2c), prevents exchange between ring conformers, and the short linker yields restricted motional position averaging resulting in a large PCS. However, the presence of isomers is still of major concern as it can significantly complicate the structural analyses of proteins.

In this study, we sought to determine how the rigidity affects the relative population of the isomers in solution. The ratio of SAP and TSAP isomers was determined by complexation of the parent compound, *SSSS*-*SSSS*-M4DOTMA, with the entire lanthanide series and characterization with HPLC, mass spectrometry, and NMR. The Ln-*SSSS*-*SSSS*-M8Spy species were conjugated to a ubiquitin S57C mutant, and the relative populations of the isomers were deduced based on the integrals of resonances shifted by the PCS for a particular nucleus in the protein. In fact, measuring the isomer population via PCS of the protein resonances due to the conjugation of Ln-*SSSS*-*SSSS*-M8SPy was an easier way to detect the presence of different isomers compared to the parent Ln- *SSSS*-*SSSS*-M8SPy itself. The protein resonance linewidths are not significantly affected by the presence of the lanthanide and the magnitude of PCS is not as large as for the protons on the Ln- *SSSS*-*SSSS* -M8SPy itself.

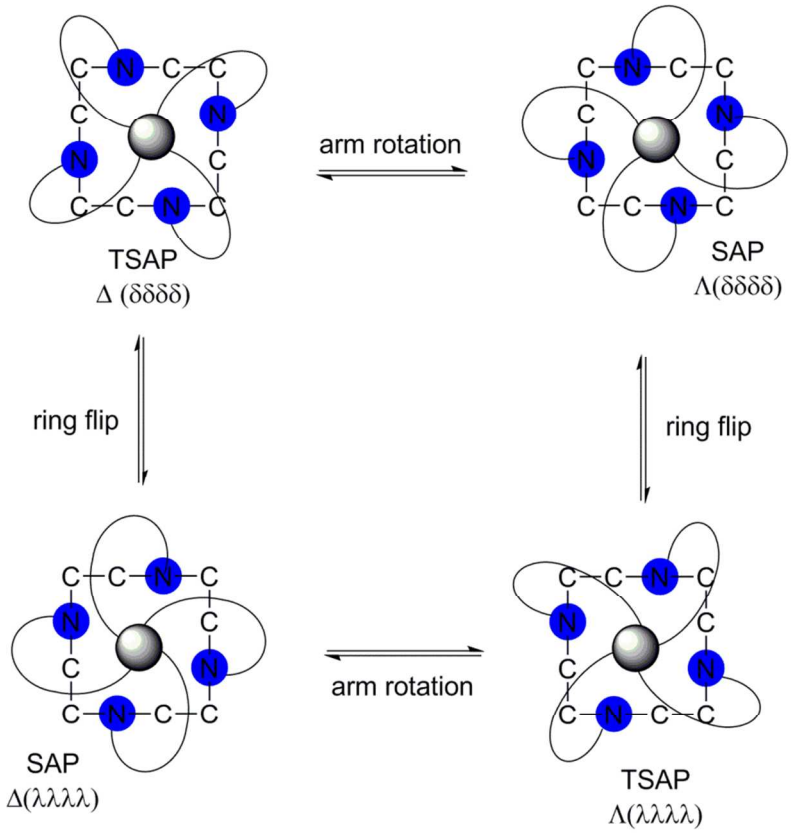

Figure 1. Schematic representation of SAP and TSAP isomer conformations for Ln-DOTA-type complexes.

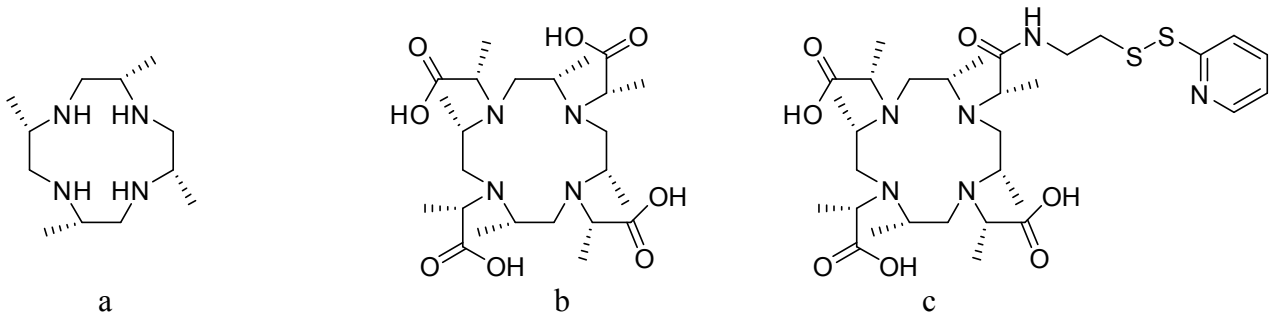

Figure 2. Chemical structures of (a) *SSSS*-M4cyclen, (b) *SSSS*-*SSSS*-M4DOTMA, and (c) *SSSS*-*SSSS*-M8SPy.

RESULTS and DISCUSSION

In this study, two methylated DOTA-type ligands were prepared, *SSSS*-*SSSS*-M4DOTMA and *SSSS*-*SSSS*-M8SPy (Figure 2b and 2c, respectively). These ligands have four ring *SSSS* methyl groups and four *SSSS* methyl substituents in the acetate arms that provide a rigid ligand framework. This molecular template is ideal for achieving restricted motion surrounding the chelated Ln^{3+}, which makes the complexes excellent sources of LIS when conjugated to macromolecules, such as proteins, and assists in the elucidation of their molecular structures in solution. The rigidification of the complex prevents fluxional averaging of the magnetic susceptibility tensor and the bulk of the ligand restricts motional averaging on the surface of the protein that would otherwise result in reduced LIS/PCS. Nevertheless, the presence of slowly exchanging isomers can lead to multiple sets of resonances that can complicate the analysis. The motivation for this work was to carefully evaluate the presence and properties of these isomers and to provide a generalized basis for application of these ligands for PCS in proteins and complexes. The characteristic isomer ratios are observable in the HSQC NMR spectrum of ubiquitin when the lanthanide complex is covalently bound to the protein.

The previous report of Haussinger and co-workers assumed that the ligand was rigid and had only one stereoisomer for the Lu^{3+} complex, based on NMR studies [22]. However, we have observed that the Lu^{3+} complex, in fact, exhibits 3% of a second isomer, based on RP-HPLC. This observation prompted a closer examination of the entire series of lanthanide complexes, which showed that the complexes generally exhibit two isomers. The presence of these two isomers can be visualized using HPLC, which reveals two resolved peaks, each peak with the same mass of the complex and characteristic lanthanide isotope pattern. Interestingly, the ratio of the isomers correlates with the atomic radius of the lanthanide ion.

The ligand, *SSSS*-*SSSS*-M4DOTMA, due to its symmetrical structure was used as the parent compound to study the isomers; while *SSSS*-*SSSS*-M8SPy, which has a pyridyl disulfide moiety on one of the pendant arms available for protein conjugation, was used to study the effect of the isomers on protein structural studies. A comprehensive discussion of the characterization of the ligand *SSSS*-*SSSS*-M4DOTMA is available in the Supporting Information.

Lanthanide *SSSS-SSSS*-M4-DOTMA studies. The ligand *SSSS-SSSS*-M4DOTMA was complexed with $LnCl_3$ (Ln^{3+} = La^{3+} - Lu^{3+}) in water at elevated temperature (343 K) while pH was maintained at 6.5. It should be noted that complexation with $LnCl_3$ in acetate buffer (pH 5.5) or the lanthanide hydroxide ($Ln(OH)_3$) form in water (pH maintained at 6.5) produced the same results. Lanthanides with larger atomic radii (La^{3+} - Sm^{3+}) took longer to complex than the smaller lanthanides (Eu^{3+}-Lu^{3+}). No complexation with La^{3+} was observed. In fact, the starting material was still present in the La^{3+} complexation reaction even after four days of stirring at 343 K. Meanwhile, full complexation was achieved within 24 hours using the rest of the lanthanide ions. The complex formation was monitored using LC-MS at 210 nm. The complexation reaction mixture was analyzed with RP-HPLC and generally exhibited two peaks with retention times of 4.30 (peak A) and 5.10 min (peak B). Isolation of each peak, followed by repeated chromatography, led to interconversion of the isomers to the equilibrium populations, indicating a dynamic equilibrium in solution. This is common for lanthanide DOTA-type complexes, which exist as two isomers, SAP and TSAP, in solution. Interconversion is quite slow, taking approximately 4 hours after dissolution for the isomers to reach equilibrium at 298 K (pH 6.5), especially for the middle lanthanides such as Ho^{3+} and Dy^{3+}. The distribution of the isomers was determined by manual integration of the HPLC peaks. The relative ratios observed are shown in Table 1.

Table 1. Relative ratios of the two isomers of lanthanide-*SSSS-SSSS*-M4DOTMA and lanthanide-*SSSS-SSSS*-M8SPy complexes observed in RP-HPLC at 298 K and pH 6.5.

	Ln-*SSSS-SSSS*M4DOTMA		Ln-*SSSS-SSSS*-M8SPy	
Ln^{3+} ion	**Peak A Λ(δδδδ)** t_R=4.30 min	**Peak B Δ(δδδδ)** t_R=5.10 min	**Peak A Λ(δδδδ)** t_R = 5.00 min	**Peak B Δ(δδδδ)** t_R = 5.40 min
La	-	-	98	2
Ce	99	1	98	2
Pr	99	1	98	2
Nd	99	1	-	-
Sm	99	1	-	-
Eu	95	5	-	-
Gd	92	8	75	25
Tb	85	15	80	20
Dy	70	30	73	27

Ho	35	65	56	44
Er	16	84	23	77
Tm	7	93	9	91
Yb	4	96	5	95
Lu	3	97	3	97

One of the isomers, which eluted first from the HPLC column (peak A), is predominant in larger lanthanides (from Ce^{3+} to Sm^{3+}). As the ionic radius decreases from Eu^{3+} to Dy^{3+}, the proportion of peak A steadily decreases, until a tipping point at Ho^{3+} where peak B becomes the major isomer. From Tm^{3+} to Lu^{3+}, it is predominantly peak B that can be observed in the chromatogram. The ratio of the signal intensities was invariant to the use of different C18 columns (Eclipse XDB-C18, Eclipse Plus C-18 and SB-C18) and different mobile phase conditions (i.e., acetonitrile/water with no TFA, with 0.05 and 0.1% TFA).

NMR studies were conducted to assign the two peaks observed from HPLC to the SAP and the TSAP isomers. The ax_1 protons from the macrocycle experience the largest hyperfine shift in Ln-DOTA-type complexes, and can easily be distinguished from the ^{1}H-NMR spectrum. The ax_1 proton of the SAP isomer has a larger paramagnetic shift than the ax_1 proton of the TSAP isomer due to larger susceptibility anisotropy [7, 23], and can therefore allow the assignment of the two isomers to their coordination geometries.

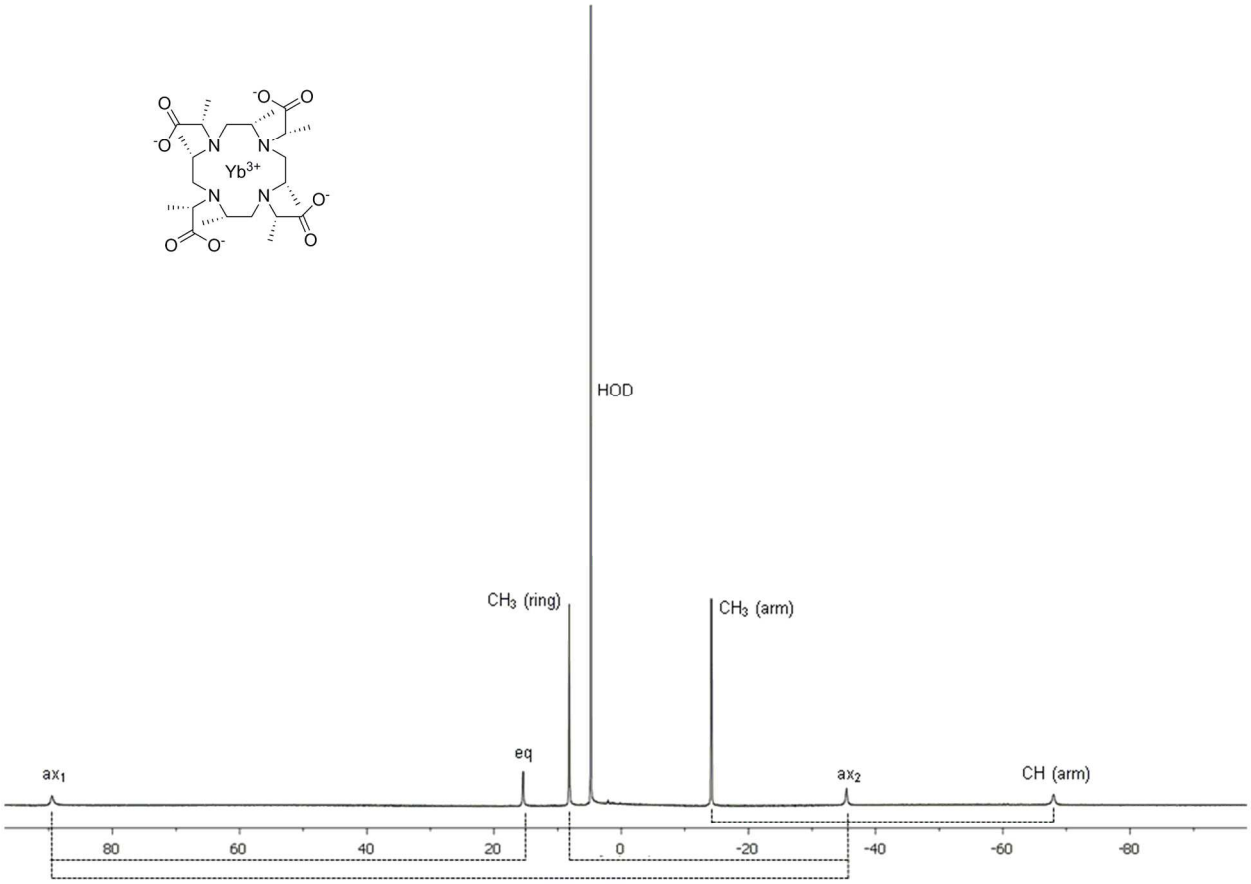

Figure 3. Proton NMR of Yb-*SSSS*-*SSSS*-M4DOTMA at 298 K and 400 MHz. The lines underneath the spectrum indicate the couplings determined from 2D COSY spectrum.

The HPLC of the Yb^{3+} complex of *SSSS*-*SSSS*-M4DOTMA (Fig. S8a) at 298 K shows that the majority of the isomer eluted at a later retention time (t_R = 5.10 min), which indicates that it exists predominantly in one isomer form. Indeed, a single isomer with six magnetically non-equivalent protons was observed in the ^{1}H NMR spectrum of the Yb^{3+} complex (Fig.3) at 298 K. The ^{1}H-NMR spectrum spans approximately 160 ppm and the peak assignments were made by comparing the resonance frequencies of the corresponding Yb-*RRRR*-DOTMA complex [24], with confirmation from a COSY spectrum (Fig. S9). There are three peaks that are readily distinguishable from the NMR spectrum: the ax_1 protons which are the most shifted proton in the spectrum (89.5 ppm), and the two methyl protons, which exist as two intense peaks at 8.2 and -14.2 ppm. From the COSY spectrum, the ax_1 protons have a strong cross-peak at 15.4 ppm that shows no connection with other resonances. This cross-peak indicates a geminal coupling and

can be assigned to the eq proton. Another cross-peak from the ax_1 protons, which is relatively weaker, can be found at -35.4 ppm, which then has a COSY connection with an intense peak at 8.2 ppm. The -35.4 ppm peak is therefore a vicinal proton (ax_2), while the 8.2 ppm peak is the ring methyl group. Coupling between the CH arm and CH_3 arm protons can easily be identified as a cross-peak between -67.9 ppm and -14.2 ppm, respectively.

The ring methyl group is located in the equatorial position as deduced from the ligand conformation, and can have two possible positions relative to the macrocycle, the "equatorial upper" and the "equatorial lower". As a reference, Figure 4 (top) shows the orientation of the protons in a macrocycle without any substituent. In the equatorial upper position, the methyl group replaces the eq_2 hydrogen in an unsubstituted macrocycle, and is on the same carbon as the ax_2 proton. The equatorial lower, on the other hand, replaces the eq_1 proton and is on the same carbon as the ax_1 proton. Based on the COSY spectrum, the methyl ring group of Yb-*SSSS*-*SSSS*-M4DOTMA is on the same carbon as the ax_2 protons, and is therefore located in the equatorial upper position, which is in agreement with data reported by Ranganathan.[25]

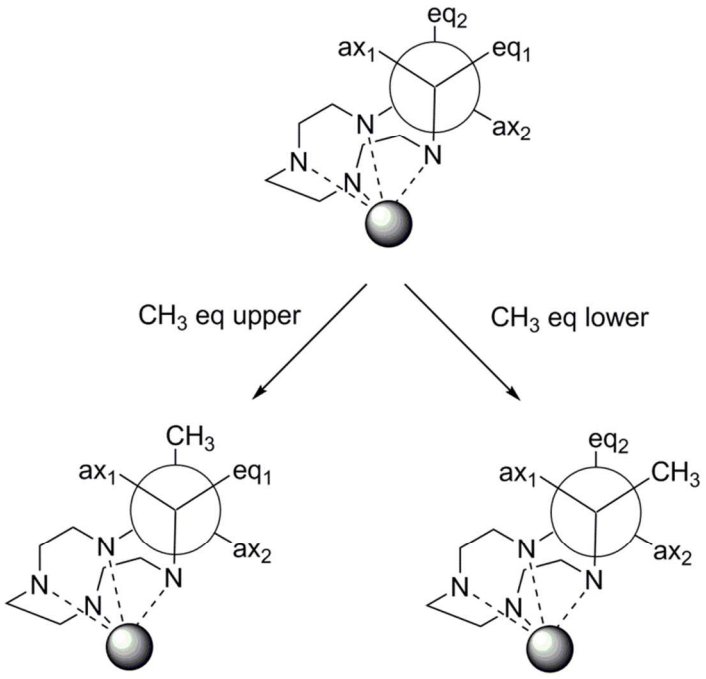

Fig.4. Possible orientations of the equatorial ring methyl group relative to the macrocycle (adapted from [16, 25]). The top portion shows the distinction of the macrocyclic protons with no

substituents. The bottom portion shows that the "eq upper" position replaces the eq_2 proton with a methyl group, while in the "eq lower", the methyl group replaces the eq_1 proton.

Based on the shifts of the ^{1}H NMR peaks, it is determined that the Yb^{3+} complex, which has the same chiralities between the macrocycle (*SSSS*) and the acetate arms (*SSSS*), adopts the TSAP configuration. Ytterbium complex of DOTMA was also reported to exist almost exclusively as TSAP isomer [26], as well as Lu-*SSSS*-*SSSS*-M8SPy (small lanthanide next to Yb^{3+}) which has the same chiralities in both the arms and the ring [22]. In contrast, Yb-*SSSS*-*RRRR*-M4DOTMA, which has two opposite chiral centers between the ring (*SSSS*) and pendant arms (*RRRR*) was reported to arrange in an SAP fashion [25]. This observation clearly shows that the chirality between the ring and the arm has a significant effect on the coordination isomers.

The same observation was reported by Woods and co-workers on 2-(*p*-nitrobenzyl)-DOTMA complexes, which bears a p-nitrobenzyl group in one of the ethylene bridges of the macrocycle. The same chirality of the ring and pendant arms (Yb-*S*-*SSSS*-NO_2BnDOTMA) leads to a TSAP geometry, while opposite chiralities (Yb-*S*-*RRRR*-NO_2BnDOTMA) result in SAP configuration [11].

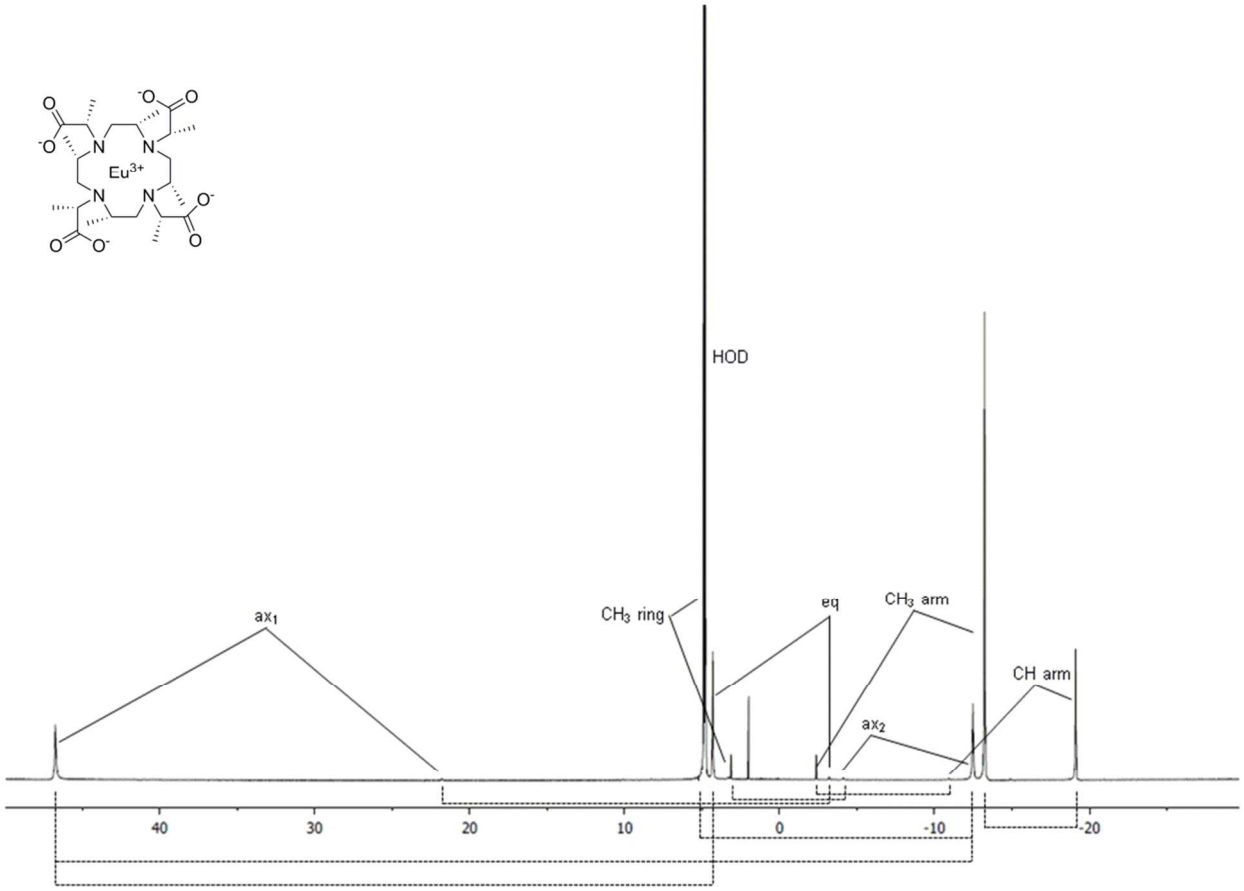

Fig. 5. Proton NMR of Eu-*SSSS*-*SSSS*-M4DOTMA) in D_2O (pH 6.5) at 298 K and 400 MHz. The lines underneath the spectrum indicate the couplings determined from 2D COSY spectrum.

The Eu^{3+} complex of *SSSS*-*SSSS*-M4DOTMA showed two peaks in the RP- HPLC chromatogram at 95:5 ratio (peak A:B; Fig S8b).The presence of two species in solution was confirmed by ^{1}H NMR, where two sets of resonances with different intensities were observed (Fig. 5). Each set has six magnetically non-equivalent protons typical for a complex of four-fold symmetry. The resonance frequency of the ax_1 protons of the major peak is at 46.7 ppm, while the ax_1 of the smaller peak can be found at 21.8 ppm. As a reference, the Eu-DOTA ax_1 protons for the SAP isomer usually reside in the 31-38 ppm region, while the TSAP isomer protons are more shifted upfield and reside in the 10-14 ppm region [23, 27, 28]. For Eu-DOTA bearing an α-substituted group on the pendant arms, the ax_1 protons are typically found between 34 and 43 ppm for the SAP isomer, and between 15 and 22 ppm for TSAP isomer [11, 14, 29]. This result suggests that the major peak in Eu-*SSSS*-*SSSS*-M4DOTMA solution is the SAP isomer, while

TSAP is the minor isomer. This observation is in contrast to the Eu-*S*-*SSSS*-DOTMA observed by Woods et al. where the same arm and ring configuration led to a predominantly TSAP configuration [29]. The peak assignments were based on 2D COSY NMR (Fig. S10). Since the ring methyl occupies the equatorial position of one of the carbons from the ethylene bridge, the ax_1 proton experiences two J-couplings to other protons: a strong geminal coupling between ax_1-eq, and vicinal coupling between ax_1-ax_2. The COSY spectrum shows that the ax_1 protons have a strong COSY connection at 4.3 ppm and a weak coupling with a peak at -12.4 ppm, which in turn has a cross-peak with one of the intense peaks at 4.8 ppm. We can therefore readily identify the shifts at 4.3 ppm to be the geminal proton (eq), the -12.4 ppm peak to be the vicinal proton (ax_2) and 4.8 ppm signal to be the ring methyl group. Finally, a cross-peak between –19.1 ppm and the other intense peak at -13.2 ppm is evident in the spectrum and is easily assigned as the CH_3 arm and CH arm protons, respectively. The same COSY pattern was found for the minor isomer. The ratio of the ax_1 protons for SAP:TSAP is 98:2, which is very close to the HPLC integration of peaks A:B (95:5). The same ratio was also found for the signal intensities of the more intense CH_3 arm proton resonances for both the SAP and TSAP isomers of Eu-*SSSS*-*SSSS*-M4DOTMA. Similar to Yb-*SSSS*-*SSSS*-M4DOTMA, the methyl ring group is linked to ax_2 protons and is oriented in the "equatorial upper" position.

In order to better understand the interconversion of the two isomer populations of Eu-*SSSS*-*SSSS*-M4DOTMA, variable-temperature ^{1}H NMR spectra were recorded over the range 298-353 K. Figure 6 reports the position and relative intensities of the twelve resonances corresponding to the two isomers. The minor isomer (TSAP) of the Eu-*SSSS*-*SSSS*-M4DOTMA complex, which is present at 2% at 298 K, allows easy monitoring of the characteristic ax_1 protons. The shifts of ax_1 protons (46.7 ppm for the SAP isomer and 21.8 ppm for the TSAP isomer) decreases with increasing temperature as well as a difference in the separation between the two peaks, which is attributed to the inverse correlation of dipolar and contact contributions to LIS with temperature. It's noticeable that the population of the minor TSAP isomer significantly increases with temperature (2% at 298 K versus ~18% at 353 K). Even though ax_1 proton resonances did broaden at higher temperature, no coalescence was observed due to a rigid complex structure. Presumably, it indicates that at higher temperatures the isomer interconversion becomes faster and approaches an intermediate exchange rate on the NMR time scale. This is in marked contrast to lanthanide DOTA chelates, which rapidly exchanges between two conformers leading to

broadening and eventual coalescence of the peaks at increasing temperature.[7] Out of the two dynamic processes (ring flip and arm rotation), it was established that isomer interconversion happens through arm rotation in this rigid ligand framework.[16, 25] The increase of the minor isomer population with temperature indicates that an energy barrier exists between SAP and TSAP isomers of the Eu-*SSSS*-*SSSS*-M4DOTMA complex. Interestingly, Haussinger reported a second set of shifted resonances for the Dy-M8SPy tagged-ubiquitin that increases in contribution to 50 % when the temperature is increased from 298 K to 323 K.[22] As demonstrated by the Eu-*SSSS*-*SSSS*-M4DOTMA, the change in the population of Dy-M8SPy-tagged ubiquitin at increasing temperature can very well be due to a change in the isomer population.

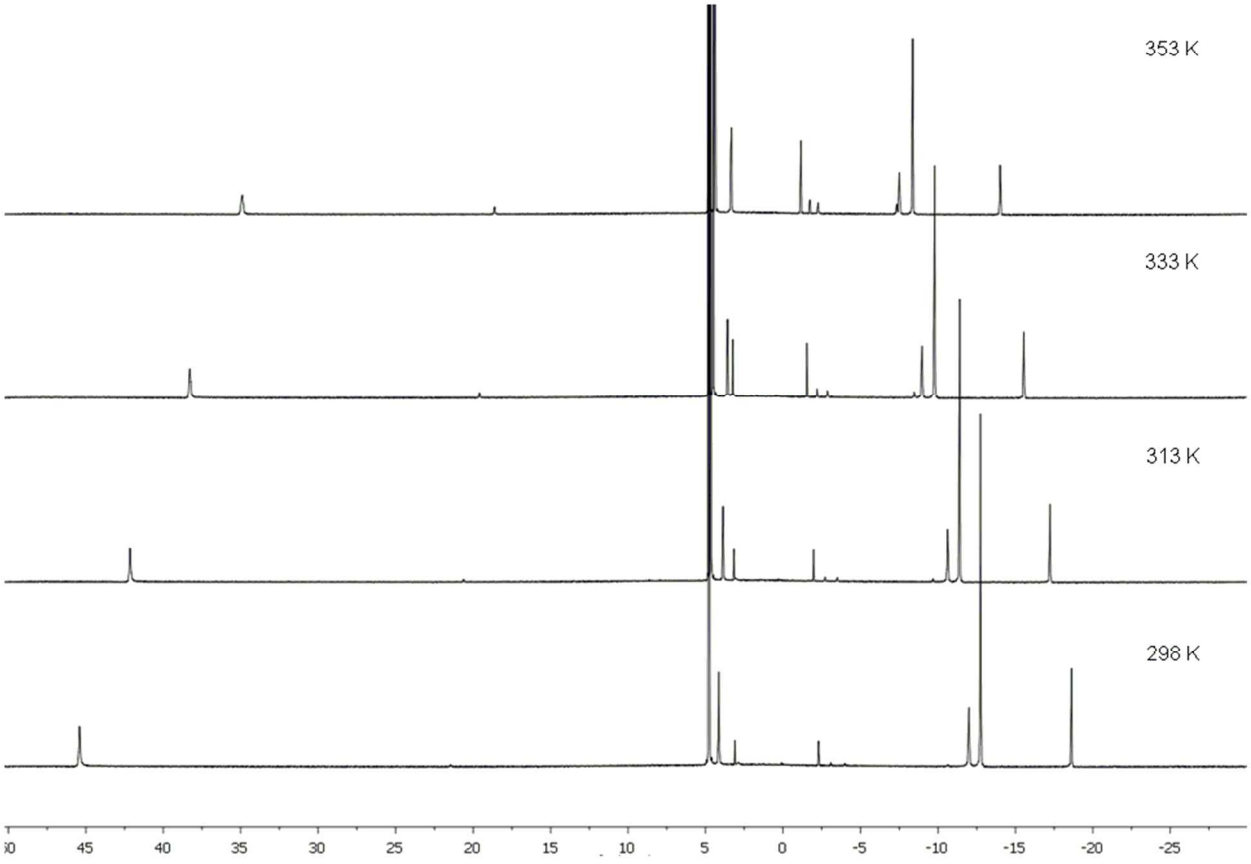

Figure 6. Variable-temperature ^{1}H NMR spectra for Eu-*SSSS*-*SSSS*-M4DOTMA at 400 MHz.

For large lanthanide chelates, such as Pr-*SSSS*-*SSSS*-M4DOTMA, the majority of the complex (99%) eluted at 4.30 min (Fig. S8c). The ^{1}H NMR spectrum at 298 K is presented in Figure 7 and

shows six major resonances from six magnetically non-equivalent protons, typical for a complex of four-fold symmetry. The proton assignments for this major species were based on the 2D COSY NMR (Fig. S11). Similar to Eu- and Yb-*SSSS*-*SSSS*-M4DOTMA, the methyl ring group of Pr-*SSSS*-*SSSS*-M4DOTMA is linked to ax_2 protons and is therefore oriented in the "equatorial upper" position. No additional peaks were observed beyond the most-shifted protons (ax_1) at -57 ppm after prolonged scanning times. However, a second set of peaks that spans 60 ppm were observed. The most shifted protons from this species can be found at -28 ppm, which is twice the magnitude of the ax_1 proton of the major isomer. It is to be noted that the more compact SAP isomer has a characteristically more shifted ax_1 protons than the TSAP geometry. To further examine these minor peaks, a 2D COSY NMR spectrum was obtained from a 600 MHz NMR spectrometer equipped with a cryoprobe at 30^{o}C (Figure S12). The most shifted peak at -28 ppm (ax_1 of minor isomer) has a COSY connection to a peak at -0.46 ppm leading to the assignment of the latter as the eq proton. Another COSY cross-peak at 17.3 ppm and 14.3 ppm can be attributed to the CH arm and CH_3 arm, respectively. A peak at -0.51 ppm that is very close to the eq proton, has a COSY connection to a small peak at 18.2 ppm. These peaks can be assigned to the protons of the CH_3 ring and ax_2, respectively. The eq and CH_3 ring of the minor isomers are slightly overlapping as can be seen by the presence of a shoulder in the proton NMR. Based on the observed chemical shifts of these isomers, it is concluded that the major isomer found in Pr-*SSSS*-*SSSS*-M4DOTMA is the SAP isomer.

Such an unusual preference of the Pr^{3+} complex to adopt the presumably SAP conformation (99 % of the SAP isomer at 298 K) prompted us to acquire variable-temperature ^{1}H NMR and EXSY spectra. The variable-temperature ^{1}H NMR spectra of Pr-*SSSS*-*SSSS*-M4DOTMA were recorded over the range 298-353 K and are presented in Figure 8. The temperature dependence of chemical shifts and broadening phenomena are similar to those observed for Eu-*SSSS*-*SSSS*-M4DOTMA. As temperature increases the peak at -28 ppm becomes more pronounced. The energy barrier observed between the rigid SAP and TSAP isomers for Eu-*SSSS*-*SSSS*-M4DOTMA also applies for Pr-*SSSS*-*SSSS*-M4DOTMA.

The EXSY spectrum was obtained to confirm that the two species are in exchange. Figure 9 shows exchange peaks between the CH_3 arm of the major and minor isomers (21.9 ppm/14.3 ppm), as well as the CH arm of the major and minor isomers (20.6 ppm/17.3 ppm). In addition,

the ax_2 of the major isomer has an exchange peak at 18.2 ppm that corresponds to ax_2 of the minor isomer. Another set of exchange peaks can be found for the eq protons of the major and minor isomer, as well as the CH_3 ring of both isomers. Finally, the exchange peak for the most shifted ax_1 protons for both isomers is observed in the EXSY spectrum. The presence of NOE peaks on the major isomer is also evident in Fig. 9, and can be found between the CH arm and the eq protons, the CH arm and CH_3 ring, CH_3 arm and CH_3 ring, ax_1 and CH_3 ring, and the eq protons and CH_3 ring, which are in excellent agreement with the optimized structure of the SAP isomer of Pr-*SSSS*-*SSSS*-M4DOTMA in Fig. 10. These interatomic H-H distances range from (2.10 A to 2.44 Å) Furthermore, the average CH arm – CH_3 ring distance of the SAP isomer is 2.44 Å as compared to that of the TSAP (4.06 Å), and thus the CH arm – CH_3 ring NOE peak in Fig. 9 can only be attributed to the SAP isomer. This provides direct evidence of the more stable SAP Pr-*SSSS*-*SSSS*-M4DOTMA in solution.

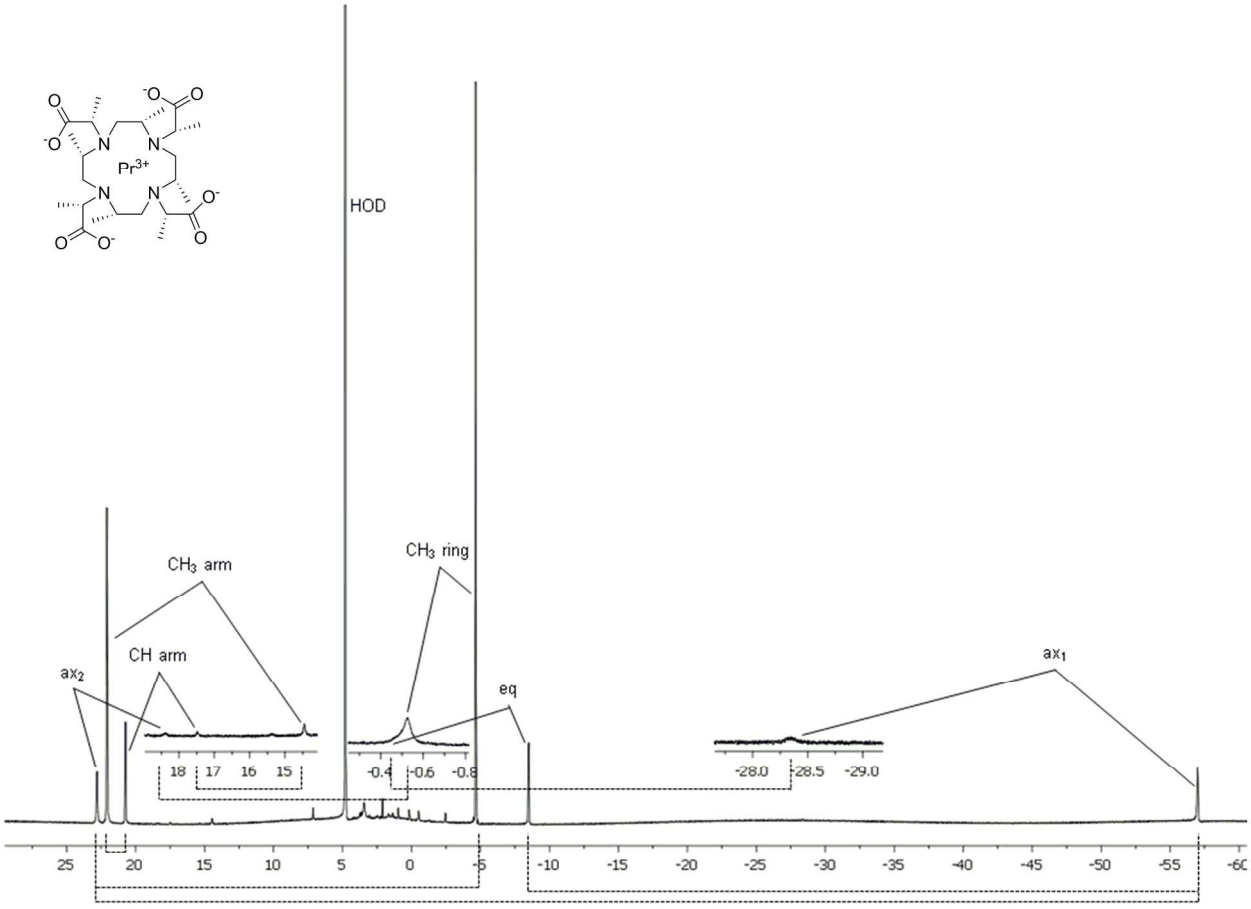

Figure 7. Proton NMR spectrum of Pr-*SSSS*-*SSSS*-M4DOTMA at 298 K (pH 6.5) and 400 MHz. The lines underneath the spectrum indicate the couplings determined from 2D COSY spectrum. The inset provides a closer view of the minor isomer of Pr-*SSSS*-*SSSS*-M4DOTMA.

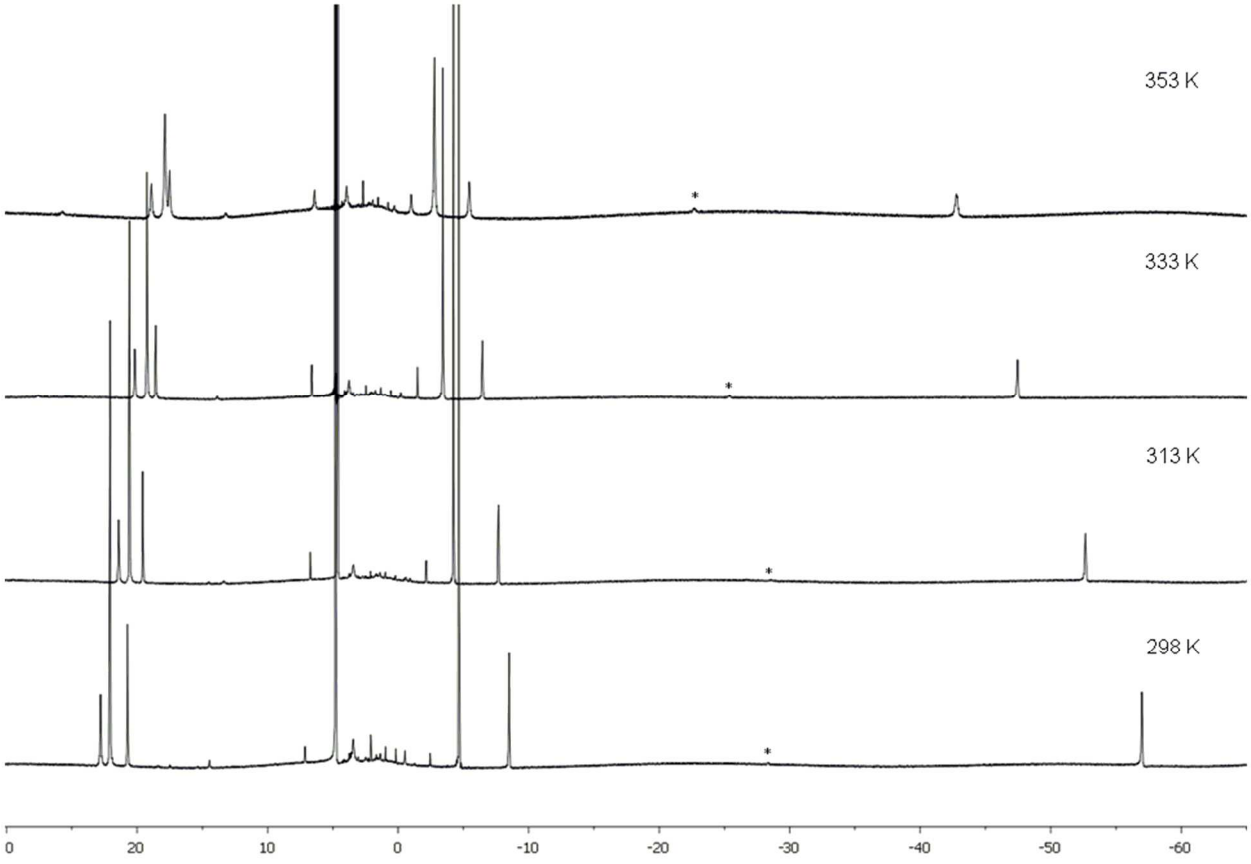

Figure 8. Variable temperature ^{1}H NMR spectra for Pr-*SSSS*-*SSSS*-M4DOTMA at 400 MHz. The asterisk shows the location of the ax_1 proton of the minor isomer.

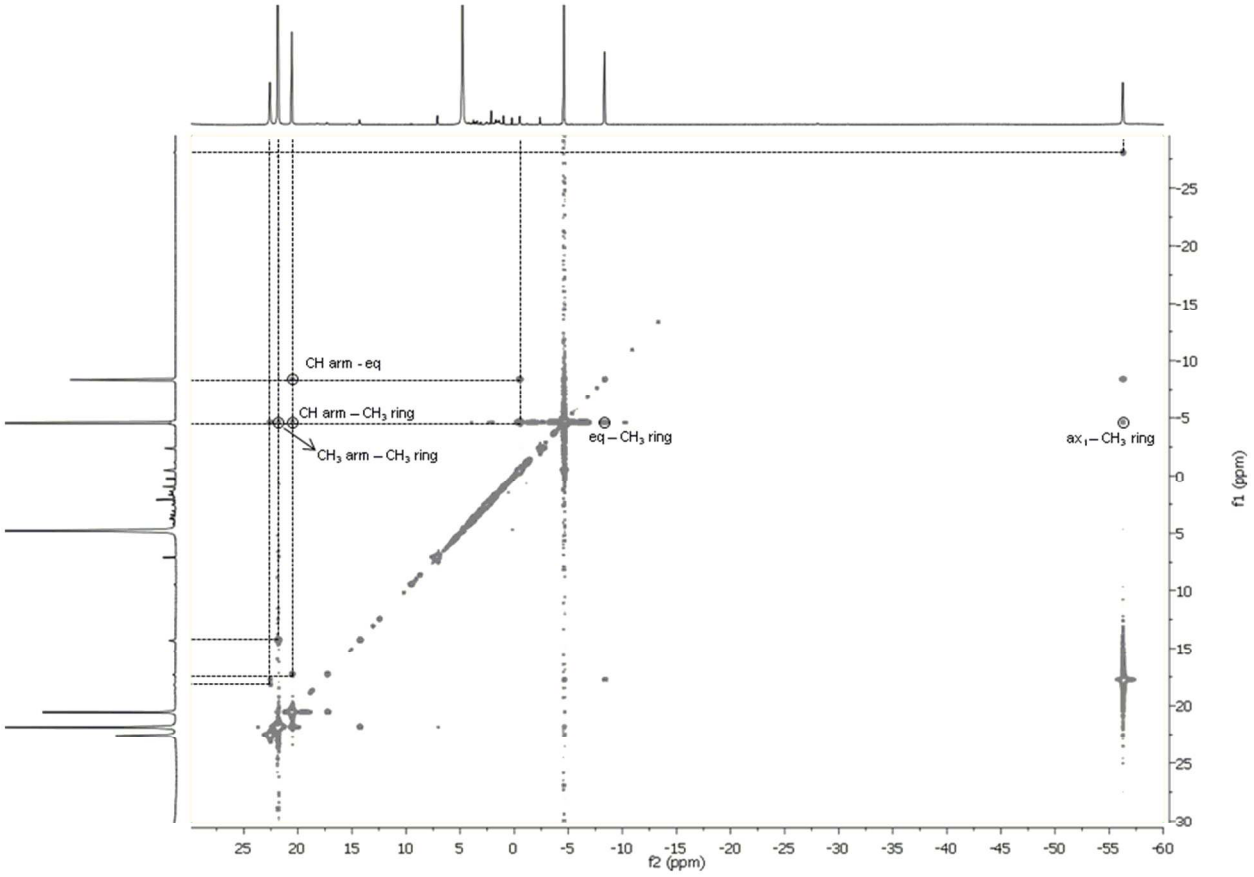

Figure 9. ^{1}H NMR EXSY spectrum of Pr-*SSSS*-*SSSS*-M4DOTMA at 30^{o}C and 600 MHz (mixing time = 25 ms) showing the correlation between the two isomers. The dashed lines link two resonances that are connected by exchange cross-peaks. The NOE peaks are encircled.

The isomeric ratio of Ln-DOTA complexes has been reported [7, 23, 27], and shows that the early lanthanide ions prefer the more open TSAP coordination. As the lanthanide ions become smaller, the SAP coordination becomes more preferred until Er^{3+} is reached, then the TSAP geometry becomes more favorable and is believed to lose its bound water molecule as the lanthanide ion size decreases. For Ln-*RRRR*-DOTMA, on the other hand, δ-substitution of the pendant arms leads to a noticeable preference for the TSAP isomer across the lanthanide series, and is adopted exclusively by the early lanthanides [26]. The SAP isomer gradually increases to no more than 30% between Tb^{3+} and Dy^{3+}, after which the TSAP becomes more favored until it reaches Yb^{3+} and Lu^{3+} where the isomer becomes almost exclusively TSAP.

In this work, a different trend is observed: the early lanthanides of *SSSS*-*SSSS*-M4DOTMA exclusively adopt the SAP geometry at room temperature, and as the lanthanide ion decreases in size, the TSAP population increases steadily until the isomers become almost exclusively TSAP as it reaches the smallest Ln^{3+} ions, Yb^{3+} and Lu^{3+}. The preference for a SAP configuration in the early lanthanides is unusual as the larger lanthanides prefer the more open TSAP geometry in other DOTA-related compounds. However, in this rigidified ligand, the presence of the *SSSS*-methyl substituents on both the arm and the ring can cause methyl-methyl repulsion that destabilizes the TSAP isomer.

Quantum chemical calculations were performed to determine the isomer stabilities, starting from the X-ray structure of Bi-DOTA, the size of which is very close to that of La^{3+} [30]. These calculations were done on the triplet ground state of the anionic Pr-DOTA, and the calculated bond lengths were compared to those in the reported X-ray structure (Table S1) [31]. The average distances calculated for Pr−N (2.732 Å) and Pr−O (2.426 Å) in the SAP form of Pr-DOTA are in good agreement with the bond distances from the X-ray structure, 2.720 Å and 2.453 Å, respectively (Table S1). Moreover, our Gibbs free energy calculations at 289.15 K indicate that the TSAP Pr-DOTA is more stable than the SAP by 1.8 kcal/mol, which is also in agreement with the experimental observation [7]. This comparison justifies the use of our theoretical approach in investigating the geometry and energetics of both Pr-*SSSS*-*SSSS*-M4DOTMA and Yb-*SSSS*-*SSSS*-M4DOTMA whose X-ray structures are not known.

It was observed that the average Pr-N distance (2.782 Å) for the SAP Pr-*SSSS*-*SSSS*-M4DOTMA is 0.05 Å longer than that of the SAP Pr-DOTA, while the corresponding Pr-O distance differs only by 0.01 Å. This indicates that the methyl groups in the macrocyclic ring are likely to cause a stronger steric repulsion than those of the pendant group, resulting in the elongation of the Pr−N distance. In both Pr-*SSSS*-*SSSS*-M4DOTMA and Yb-*SSSS*-*SSSS*-M4DOTMA, the Ln-N distance of the TSAP conformer is calculated to be shorter than that of the SAP by at least 0.025 Å. It is further noted that our calculated structures of Yb-*SSSS*-*SSSS*-M4DOTMA (Figure 10) have the methyl ring on the equatorial upper position consistent with the observed NMR spectra.

Our experiments indicate that the SAP of Pr- *SSSS*-*SSSS*-M4DOTMA is more stable than TSAP by at least 2.7 kcal/mol in terms of the relative Gibbs free energy (ΔG). However, the quantum chemical calculations suggest that while the SAP isomer of Pr- *SSSS*-*SSSS*-M4DOTMA is more stable than TSAP as to both relative electronic energy (ΔE = 1.8 kcal/mol) and enthalpy (ΔH = 1.2 kcal/mol), it becomes less stable in terms of ΔG by 1.1 kcal/mol. This is due to the fact that the TSAP has a higher calculated vibrational entropy stemming from the low vibrational frequencies (< 620 cm^{-1}) as compared to the SAP.

In the case of Yb- *SSSS*-*SSSS*-M4DOTMA, the TSAP is more stable than the SAP in terms of ΔE, ΔH, and ΔG. Our experiments suggest that the TSAP form is more stable by ΔG of 1.8 kcal/mol, and this is in good agreement with the calculated ΔG of 2.1 kcal/mol. The computed structures of both the Yb- and Pr- *SSSS*-*SSSS*-M4DOTMA are presented in Fig. 10.

The NMR results conclude that peak A is the complex with a SAP configuration while peak B is the complex with a TSAP configuration. The observation of the SAP and TSAP isomers using HPLC was reported in Gd-pSCN BnDOTA and Eu-pNO2- BnDOTA [32], however this is the first report that studied the interconversion of isomers across the lanthanide series using HPLC. The use of different types of C18 columns and mobile phase conditions (with and without TFA) did not change the elution profile of the isomers. It is possible that SAP, being the more compact isomer is also the more hydrophilic between the two.

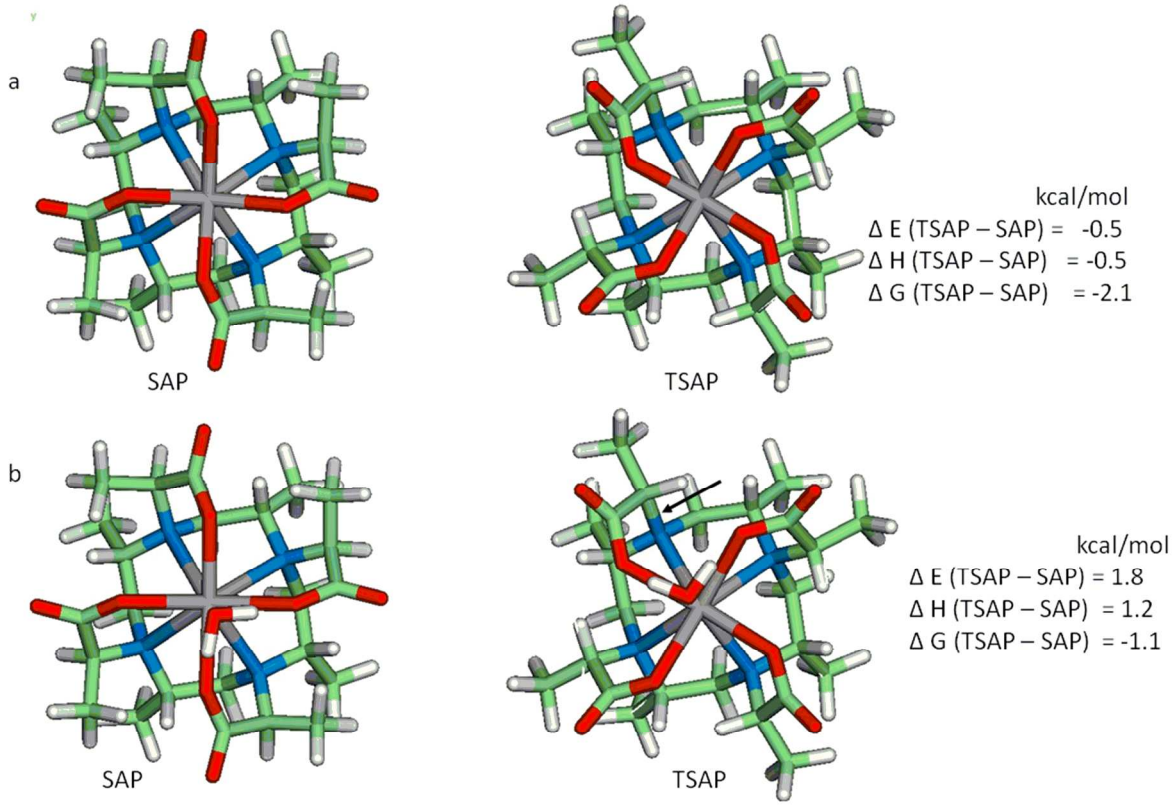

Fig. 10. Geometry optimized conformers of (a) Yb- *SSSS*-*SSSS*-M4DOTMA and (b) Pr- *SSSS*-*SSSS*-M4DOTMA at the level of MO6L functional with the pseudopotential SDD for the Pr^{3+} and Yb^{3+} atoms and the 6-31+G* basis set for the rest of the atoms. The ΔH and ΔG were calculated at 298.15 K in the reaction field of water utilizing the polarizable continuum model. For the anionic Pr-*SSSS*-*SSSS*-M4DOTMA, single point energy calculations were done on the triplet-state based on the singlet state optimized geometry. Each of the pendant carboxylate arms was rotated with respect to the C-N bond as indicated by the arrow to convert TSAP to SAP. Atoms are colored as follows: white, hydrogen; green, carbon; blue, nitrogen; red, oxygen; gray, Pr^{3+} and Yb^{3+}. The coordinates for these Ln-complexes are available in the Supporting Information (Table S2-S7).

Lanthanide-*SSSS*-*SSSS*-M8SPy studies. The ligand designed for coupling to proteins, *SSSS*-*SSSS*-M8-SPy (Fig. 2c), differs from *SSSS*-*SSSS*-M4DOTMA only in the modification of one arm. Hence, it would be anticipated to exhibit similar isomer behavior and the series of Ln-*SSSS*-*SSSS*-M8SPy was investigated. The synthesis of *SSSS*-*SSSS*-M8SPy was performed according to reported procedures [22] and was obtained with comparable yields. The complexation

of *SSSS*-*SSSS*-M8SPy with lanthanide chloride was performed in a 0.100 M acetate buffer (pH 5.50) at 348 K, and was monitored using LC-MS, by observing the appearance of the complex (t_R = 5.00 and 5.40 min) and the disappearance of the ligand peak (t_R = 5.50 min) (Fig. S13 a. ligand, b. Dy- *SSSS*-*SSSS*-M8SPy, c. Ho- *SSSS*-*SSSS*-M8SPy, d. Yb- *SSSS*-*SSSS*-M8SPy, e. Pr-*SSSS*-*SSSS*-M8SPy). During complexation with the larger lanthanides (La^{3+} - Sm^{3+}), it was observed that the ligand started to hydrolyze before the complex fully formed, however, complete complex formation was achieved using Gd^{3+} to Lu^{3+} metals. Hydrolysis was characterized by a loss of m/z of 110 pertaining to hydrolysis of the pyridyl disulfide group. Despite the hydrolysis mixture, the fully formed complexes of the larger lanthanides (La^{3+}-Pr^{3+}) with pyridyl disulfide were isolated by semi-preparative RP-HPLC. The isomer ratios were observed at 254 nm, 298 K and are shown in Table 1.

The ratios are similar to that of Ln-*SSSS*-*SSSS*-M4DOTMA, except that the change in trend, for Ln-*SSSS*-*SSSS*-M8SPy is at Er^{3+} instead of Ho^{3+} for Ln-*SSSS*-*SSSS*-M4DOTMA where peak B becomes the major isomer, which can be due to the change in one of the pendant arms to an amide substituent.

The HPLC profile of Pr-*SSSS*-*SSSS*-M8SPy showed that the majority of the complex eluted as Peak A (5.00 min), consistent with our observation for Pr-*SSSS*-*SSSS*-M4DOTMA (Fig. S13e). The COSY spectrum was then obtained to assign the proton peaks (Fig. S14). Similar to Ln-*SSSS*-*SSSS*-M4DOTMA studied earlier, the methyl ring substituent is located in the equatorial upper position. The NOESY spectrum of Pr-*SSSS*-*SSSS*-M8SPy (Fig. S15) shows cross-peaks between the CH_3 ring and the CH_3 arm, and between the eq protons and the CH_3 ring. The other NOESY peaks observed for Pr-*SSSS*-*SSSS*-M4DOTMA were not detected for Pr-*SSSS*-*SSSS*-M8SPy, perhaps due to the asymmetric nature of the complex leading to a loss of sensitivity. Most notable in the NOESY spectrum is a coupling between the CH_2 proton (3.15 ppm) of the pendant arm bearing the pyridine ring and the protons from one of the CH_3 arms (21.98 ppm). As illustrated in Fig. S15 using the optimized structure of Pr-*SSSS*-*SSSS*-M8Spy in the SAP configuration, these two protons are in close proximity (2.20 Å). This NOE is not possible with the TSAP where the distance between the two protons is >4.64 Å (Fig. S15). Given the flexibility of the pyridyl substituent, neither of these two energy-optimized isomers may represent a global minimum. Nevertheless, the energetics based on the singlet state optimized

structures in the gaseous phase indicate that the SAP isomer is more stable than the TSAP by ΔG of 1.4 kcal/mol at 298.15 K. The NOE of Pr-*SSSS*-*SSSS*-M8SPy was further compared to the Yb-*SSSS*-*SSSS*-M8SPy, which predominantly exists as a TSAP isomer. Both the COSY (Fig. S16) and the NOESY (Fig. S17) spectra were taken. The same couplings between the CH_3 ring and CH_3 arm, and the eq and CH_3 ring protons were observed. As expected, based on the optimized structure of the TSAP isomer of Yb-*SSSS*-*SSSS*-M8SPy, the coupling between the CH_2 from the pendant arm with the pyridyl substituent and the CH_3 arm was not observed due to a longer distance between these two protons in the TSAP configuration (> 4.59 Å). The present NOE study together with the quantum calculations thus provides the indisputable evidence of the unusual SAP configuration of the larger lanthanide complex.

We also observed their effect on protein NMR resonances. The lanthanide complex of *SSSS*-*SSSS*-M8SPy was conjugated to ubiquitin S57C mutant by alkylating the cysteine side-chain of the protein with the pyridine disulfide group of the lanthanide complex. The control $^{1}H/^{15}N$-HSQC spectrum of free ^{15}N-ubiquitin^{S57C}, in the presence of 2 mM DTT, was identical to that of wild-type ubiquitin with the exception of one resonance peak alteration. This chemical shift change corresponded to the S57C mutation, which meant that the chemical shifts of free ^{15}N-ubiquitin^{S57C} could be unambiguously assigned from wild-type ubiquitin chemical shifts. A $^{1}H/^{15}N$-HSQC spectrum was also obtained for each of the three Ln-*SSSS*-*SSSS*-M8SPy-tagged ^{15}N-ubiquitin^{S57C} samples (Ln = Dy, Ho, and Yb) to confirm attachment of the tag and the presence of PCS (Fig. 11). Yb- *SSSS*-*SSSS*-M8SPy, Dy- *SSSS*-*SSSS*-M8SPy, and Ho-*SSSS*-*SSSS*-M8SPy species each exhibit two shifted peaks whose intensity is in agreement with the isomeric populations in Table 1, which suggests that the multiple peaks are due to the isomerization of the M8SPy tag itself.

These data confirm that the isomers remain in the ligated protein and that the different isomers have different magnetic anisotropy tensors for the chelated Ln^{3+}, which give different values of the PCS for each isomer. The HSQC of Yb-*SSSS*-*SSSS*-M8SPy, on the other hand, showed one major peak for each amino acid since one isomer was dominant, as observed in the RP-HPLC chromatogram (95%).

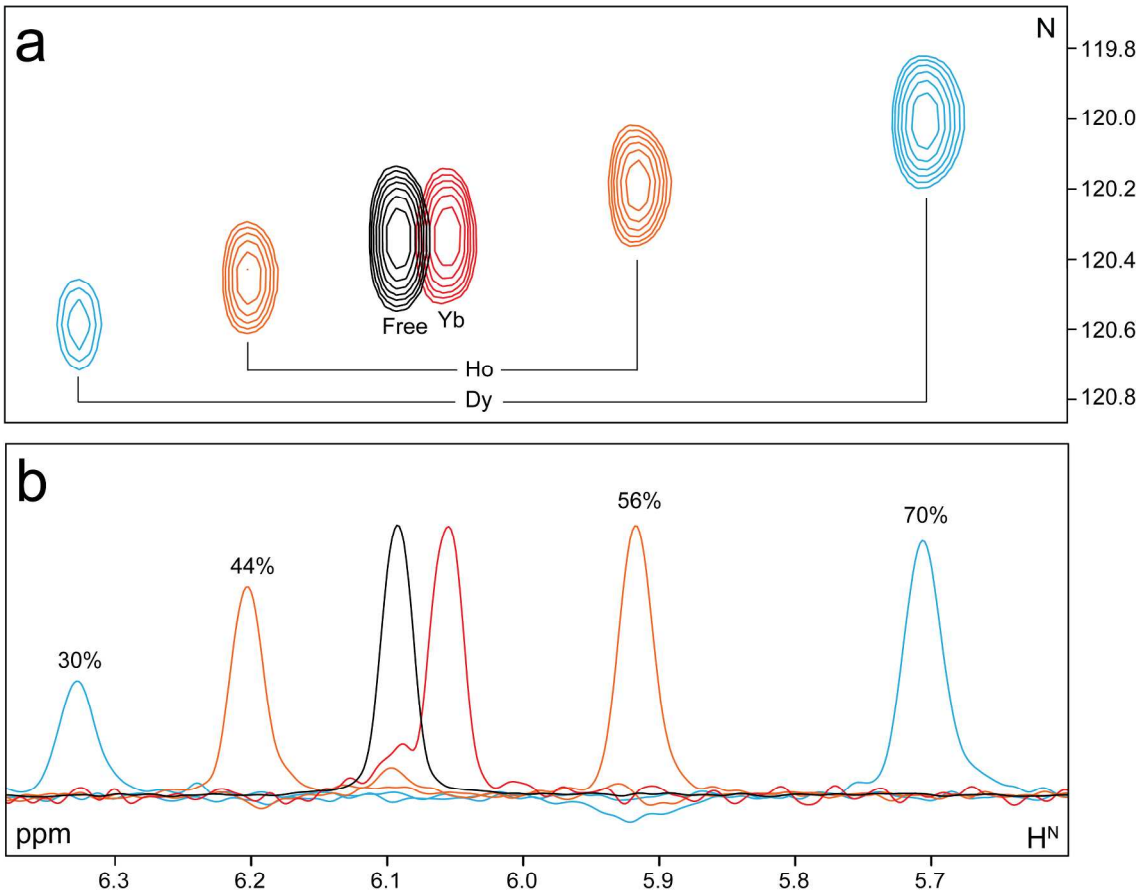

Figure 11. Pseudocontact shifts for residue I36 of Dy-, Ho-, and Yb-*SSSS*-*SSSS*-M8SPy-tagged ubiquitin^{S57C}. (a) Zoom of the $^{1}H/^{15}N$-HSQC NMR spectrum for the isolated I36 ubiquitin^{S57C} peak, highlighting the fact that pseudocontact shifts for each of the three lanthanides were in approximately the same direction, although on a different magnitude due to the difference in magnetic susceptibility between the paramagnetic metal ions. B) Horizontal traces for each of the peaks shown in (a), zero-filled for clarity. Dy- and Ho- *SSSS*-*SSSS*-M8SPy-tagged ubiquitin^{S57C} produced two peaks each, one for each isomer of the tag, which corresponded to a 3:7 ratio (Dy^{3+} in blue) and an 11:14 ratio (Ho^{3+} in orange) of peak height. Yb- *SSSS*-*SSSS*-M8SPy-tagged ubiquitin^{S57C}, in contrast, produced only one major peak (shown in red) with a

PCS since one isomer dominates. The second (minor) peak is not shown since it was barely detectable above the noise.

CONCLUSIONS

A series of lanthanide complexes of *SSSS*-*SSSS*-M4DOTMA and *SSSS*-*SSSS*-M8Spy were synthesized and their isomeric ratios were evaluated by RP-HPLC and NMR at 298 K (pH 6.5). The isomeric populations obtained by HPLC are in excellent agreement with ratios obtained by ^{1}H NMR for the europium complex of *SSSS*-*SSSS*-M4DOTMA. To the best of our knowledge, this is the first study to employ reverse-phase chromatography to evaluate the isomeric ratio of the lanthanide complexes. In the case of Yb-*SSSS*-*SSSS*-M4DOTMA complex, the HPLC analyses proved to be even more informative. Due to the lack of NMR sensitivity, the minor isomer (SAP, 4%) would otherwise be overlooked. The early lanthanides, as shown by the Pr-*SSSS*-*SSSS*-M4DOTMA, unprecedentedly favor the SAP conformation. Interestingly, the isomeric populations, which show as two sets of shifted peaks, are maintained upon covalent attachment of Dy-, Ho- and Yb- *SSSS*-*SSSS*-M8Spy complexes to the protein. The doubling of shifted resonances can be both beneficial and complicating in protein structure determination. If the set of shifted resonances can be uniquely assigned to each of the isomeric species and the PCS determined, then the availability of two tensor orientations is an advantage. However, as the size of the protein increases, the ability to resolve and assign all resonances will diminish. In such cases, the tag should be selected to induce only one set of shifted resonances. The rigidified polymethylated DOTA complexes used in this work provide a good platform to detect the presence of different isomers and can be the basis for a proper selection of lanthanide tag for protein structural studies.

EXPERIMENTAL

Analytical and semi-preparative HPLC analyses were performed on an Agilent 1200 Series instrument equipped with multi-wavelength detectors. Flash chromatography was performed on Ana-Logix IntelliFlash 280 System. Liquid chromatography- mass spectrometry (LC-MS) was performed on an Agilent 1200 Series instrument equipped with LC/MSD TrapXCT Agilent Technologies system. An Eclipse Plus C18 column (4.6 x 50 mm; 5 μm) was used. Solvent A

was 0.1% TFA in water, Solvent B was 0.1% TFA in acetonitrile, and a linear gradient of 5% B to 95% B over 8 min and further maintained for 1 min at a flow rate of 0.5 mL/min was used. UV-Vis spectrophotometry was carried out on a Perkin Elmer Lambda 25 Spectrometer. ^{1}H and ^{13}C NMR spectra were obtained on a Varian 400 MHz NMR spectrometer.^{13}C two-dimensional DEPT and COSY measurements were performed on a Varian 400 MHz NMR spectrometer using standard pulse programs. Additional ^{1}H-^{1}H COSY experiments for lanthanide-*SSSS*-*SSSS*-M4DOTMA were carried out on a Bruker 600 MHz spectrometer equipped with a cryoprobe to provide better resolution and sensitivity and processed using NMRPipe [33]. The EXSY spectrum was obtained using a Bruker 600 MHz spectrometer using the conventional NOESY pulse sequence, with a mixing time of 25 ms.

The preparation of *SSSS*-*SSSS*-M8SPy ligand was performed using the procedure reported by Haussinger et al. with similar yields [22] .

Preparation of Ln-M4DOTMA complexes. Complexation of *SSSS*-*SSSS*-M4DOTMA was performed using the method reported by Ranganathan et al. [25]. Briefly, the ligand (0.0227 mmol) was dissolved in deionized water and the pH was adjusted to ~6.5. To this was added $LnCl_3.xH_2O$; x = number of water molecules (0.227 mmol) dissolved in deionized water (2.27 mL). The pH was again adjusted to ~6.5 using 1 N NaOH. The reaction was stirred at 343 K and monitored by LC-MS. After completion, the excess lanthanide was precipitated to the corresponding $Ln(OH)_3$ by adjusting the pH to ~9 and then filtered using 0.20 µm membrane filter. The filtrate was collected and the pH was adjusted to ~7 followed by lyophilization. Purification was performed using semi-preparative HPLC over an Eclipse XDB-C18 column (9.4 x 250 mm; 5 µm). The excess lanthanide (if any) was washed with 100% water for 30 min, followed by a linear gradient of 0-95% acetonitrile for 45 min to elute the complex. The flow rate used was 2 mL/min. Removal of the excess lanthanide was monitored using xylenol orange test (UV-Vis at 350 – 700 nm) [34].

In all cases, LC-MS of the complexes gave two peaks at t_R = 4.30 and 5.10 min, and each peak exhibited characteristic lanthanide isotope pattern

Ce-M4DOTMA. *m/z* (ESI-MS +): calcd for $[C_{24}H_{42}N_4O_8Ce]^+$ $[M^{-1}+2H^+]^+$ 654.2, found 654.7

Pr-M4DOTMA. *m/z* (ESI-MS +): calcd for $[C_{24}H_{42}N_4O_8Pr]^+$ $[M^{-1}+2H^+]^+$ 655.2, found 655.7

Nd-M4DOTMA. *m/z* (ESI-MS +): calcd for $[C_{24}H_{42}N_4O_8Nd]^+$ $[M^{-1}+2H^+]^+$ 656.2, found 655.5

Sm-M4DOTMA. *m/z* (ESI-MS +): calcd for $[C_{24}H_{42}N_4O_8Sm]^+$ $[M^{-1}+2H^+]^+$ 666.2, found 666.8
Eu-M4DOTMA. *m/z* (ESI-MS +): calcd for $[C_{24}H_{42}N_4O_8Eu]^+$ $[M^{-1}+2H^+]^+$ 667.2, found 667.7
Gd-M4DOTMA. *m/z* (ESI-MS +): calcd for $[C_{24}H_{42}N_4O_8Gd]^+$ $[M^{-1}+2H^+]^+$ 672.2, found 672.6
Tb-M4DOTMA. *m/z* (ESI-MS +): calcd for $[C_{24}H_{42}N_4O_8Tb]^+$ $[M^{-1}+2H^+]^+$ 673.2, found 673.8
Dy-M4DOTMA. *m/z* (ESI-MS +): calcd for $[C_{24}H_{42}N_4O_8Dy]^+$ $[M^{-1}+2H^+]^+$ 678.2, found 677.9
Ho-M4DOTMA. *m/z* (ESI-MS +): calcd for $[C_{24}H_{42}N_4O_8Ho]^+$ $[M^{-1}+2H^+]^+$ 679.2, found 679.7
Er-M4DOTMA. *m/z* (ESI-MS +): calcd for $[C_{24}H_{42}N_4O_8Er]^+$ $[M^{-1}+2H^+]^+$ 680.2, found 680.2302*
Tm-M4DOTMA. *m/z* (ESI-MS +): calcd for $[C_{24}H_{42}N_4O_8Tm]^+$ $[M^{-1}+2H^+]^+$ 683.2, found 683.9
Yb-M4DOTMA. *m/z* (ESI-MS +): calcd for $[C_{24}H_{42}N_4O_8Yb]^+$ $[M^{-1}+2H^+]^+$ 688.2, found 688.7
Lu-M4DOTMA. *m/z* (ESI-MS +): calcd for $[C_{24}H_{42}N_4O_8Lu]^+$ $[M^{-1}+2H^+]^+$ 689.2, found 689.7
*obtained using high resolution ESI-MS

Preparation of Ln-M8SPy complexes. Lanthanide complexation of *SSSS*-*SSSS*-M8SPy was performed using Haussinger and co-worker's method [22]. Briefly, the ligand (0.102 mmol) was dissolved in 100 mM ammonium acetate buffer, pH 5.5 (6.7 mL). $LnCl_3.xH_2O$; x = number of water molecules (0.409 mmol) dissolved in the same buffer (1.8 mL) was added to the ligand solution. The reaction was stirred at 348 Kand the progress of the reaction was monitored using LC-MS at 254 nm. After completion, the sample was freeze-dried. The same purification method described earlier for Ln-*SSSS*-*SSSS*-M4DOTMA was used.

In all cases, LC-MS of the complex gave two peaks at t_R = 5.00 and 5.40 min, and each peak exhibited characteristic lanthanide isotope patterns.
Gd-M8SPy. *m/z* (ESI-MS +): calcd for $[C_{31}H_{50}N_6O_7S_2Gd]^+$ $[M+H]^+$ 840.2, found 840.4
Tb-M8SPy. *m/z* (ESI-MS +): calcd for $[C_{31}H_{50}N_6O_7S_2Tb]^+$ $[M+H]^+$ 841.2, found 841.7
Dy-M8SPy. *m/z* (ESI-MS +): calcd for $[C_{31}H_{50}N_6O_7S_2Dy]^+$ $[M+H]^+$ 846.2, found 845.6
Ho-M8SPy. *m/z* (ESI-MS +): calcd for $[C_{31}H_{50}N_6O_7S_2Ho]^+$ $[M+H]^+$ 847.2, found 847.9
Er-M8SPy. *m/z* (ESI-MS +): calcd for $[C_{31}H_{50}N_6O_7S_2Er]^+$ $[M+H]^+$ 848.2, found 848.2447*
Tm-M8SPy. *m/z* (ESI-MS +): calcd for $[C_{31}H_{50}N_6O_7S_2Tm]^+$ $[M+H]^+$851.2, found 851.7
Yb-M8SPy. *m/z* (ESI-MS +): calcd for $[C_{31}H_{50}N_6O_7S_2Yb]^+$ $[M+H]^+$ 856.2, found 856.0
Lu-M8SPy. *m/z* (ESI-MS +): calcd for $[C_{31}H_{50}N_6O_7S_2Lu]^+$ $[M+H]^+$ 857.2, found 857.7

*obtained using high resolution ESI-MS

Preparation of Ln-M8Spy ubiquitin complexes. The S57C ubiquitin plasmid was prepared using a Quik-Change site-directed mutagenesis kit (Stratagene). ^{15}N-ubiquitin^{S57C} was expressed and purified as was previously described for wild-type ubiquitin [35] but with slight alterations; ubiquitin was extracted from cells at pH 7 to allow reduction of disulfide-bonded dimers using 5 mM TCEP, the acetic acid precipitation was carried out at pH 4.3 and the purified ubiquitin was incubated with 5 mM TCEP for 30 minutes prior to size exclusion gel filtration in 50 mM sodium phosphate buffer, pH 7. Yb-, Dy- and Ho-*SSSS*-*SSSS*-M8SPy-tagged ^{15}N-ubiquitin^{S57C} were prepared as previously described [22] with the exception that 2 mM DTT was used as the reducing agent in place of TCEP so that the protein dimer reduction could be followed by NMR.

NMR spectroscopy of Ln-M8SPy-tagged ubiquitin. ^{1}H/^{15}N-HSQC NMR spectra were obtained with 32 scans and at 27 °C for each of Yb-, Dy- and Ho-*SSSS*-*SSSS*-M8SPy-tagged ^{15}N-ubiquitin^{S57C} (0.5 mM protein in 10 mM sodium phosphate, pH 6) on a Bruker Avance 600 MHz spectrometer equipped with a room temperature probe. ^{15}N-ubiquitin in the presence of 2 mM DTT was used as a control spectrum. Spectra were processed using NMRPipe [33] and assigned using CCPN Analysis [36]. Protein NMR spectra were prepared using NMRDraw [33].

Quantum Chemistry. Quantum chemical calculations with density functional theory were carried out using the MO6L functional [37] with the pseudopotential SDD [38] for 28 core electrons of the Pr^{3+} and Yb^{3+} atoms and the triple zeta basis set for their valence electrons, together with the 6-31+G* basis set for the rest of the atoms, as implemented in Gaussian 09 software [39]. The X-ray structure of Bi-DOTA [30] was used as a template to construct the structures of Pr-DOTA, Pr- *SSSS*-*SSSS*-M4DOTMA and Yb-*SSSS*-*SSSS*-M4DOTMA with the TSAP conformation. The SAP conformers were then obtained by rotating each of the four pendant carboxylate arms with respect to C-N bond as depicted in Fig.10. The geometry optimization was carried out in the reaction field of water in the presence of bound water for the anionic Pr-DOTA and Pr- *SSSS*-*SSSS*-M4DOTMA and without a bound water molecule for the anionic Yb- *SSSS*-*SSSS*-M4DOTMA. The calculations were done for the restricted singlet state for the anionic Pr-DOTA and Pr-*SSSS*-*SSSS*-M4DOTMA as well as for the unrestricted doublet state for the anionic Yb-*SSSS*-*SSSS*-M4DOTMA. For each Pr^{3+} complex, a triplet ground state was found to be more

stable than its singlet ground state. Accordingly, the triplet-state geometry optimization was carried out for the anionic Pr-DOTA. As for the anionic Pr-*SSSS*-*SSSS*-M4DOTMA, no further geometry optimization was carried out due to lack of energy convergence. Instead, single point energy calculations were done on the triplet-state based on the singlet-state optimized geometry. To facilitate the interpretation of the NOE on Pr-*SSSS*-*SSSS*-M8Spy and Yb-*SSSS*-*SSSS*-M8Spy, the geometry optimization was also done in the gaseous phase for the singlet state of Pr-*SSSS*-*SSSS*-M8Spy as well as for the doublet state of Yb-*SSSS*-*SSSS*-M8Spy. These structures were constructed by modifying a single acetate arm of the respective geometry-optimized Pr-*SSSS*-*SSSS*-M4DOTMA and Yb-*SSSS*-*SSSS*-M4DOTMA into a linear chain of a pyridyl disulfide group, as shown in Fig.2c. The coordinates for these Ln-complexes are available in the Supporting Information (Table S8-S10).

ACKNOWLEDGMENT

The quantum chemical study utilized PC/LINUX clusters at the Center for Molecular Modeling of the NIH (http://cit.nih.gov) and this research is supported by the NIH Intramural Research Program through the Center for Information Technology, NCI, and NHLBI.

REFERENCES

1. W. P. Cacheris, S. C. Quay and S. M. Rocklage, *Magnetic Resonance Imaging*, 1990, **8**, 467-481.
2. W. P. Cacheris, S. K. Nickle and A. D. Sherry, *Inorg. Chem.*, 1987, **26**, 958-960.
3. Z. Baranyai, E. Brucher, T. Ivanyi, R. Kiraly, I. Lazar and L. Zekany, *Helvetica Chimica Acta*, 2005, **88**, 604-617.
4. K. Kumar, C. A. Chang and M. F. Tweedle, *Inorg. Chem.*, 1993, **32**, 587-593.
5. J. F. Desreux, *Inorg. Chem.*, 1980, **19**, 1319-1324.
6. S. Hoeft and K. Roth, *Chem. Ber. Recl.*, 1993, **126**, 869-873.
7. S. Aime, M. Botta and G. Ermondi, *Inorg. Chem.*, 1992, **31**, 4291-4299.
8. V. Jacques and J. F. Desreux, *Inorg. Chem.*, 1994, **33**, 4048-4053.
9. S. Aime, M. Botta, G. Ermondi, E. Terreno, P. L. Anelli, F. Fedeli and F. Uggeri, *Inorg. Chem.*, 1996, **35**, 2726-2736.
10. M. Meyer, V. Dahaoui-Gindrey, C. Lecomte and L. Guilard, *Coord. Chem. Rev.*, 1998, **178**, 1313-1405.
11. M. Woods, Z. Kovacs, S. Zhang and A. D. Sherry, *Angew Chem Int Ed Engl*, 2003, **42**, 5889-5892.
12. M. Woods, M. Botta, S. Avedano, J. Wang and A. D. Sherry, *Dalton Trans*, 2005, 3829-3837.
13. F. A. Dunand, S. Aime and A. E. Merbach, *J. Am. Chem. Soc.*, 2000, **122**, 1506-1512.
14. M. Woods, S. Aime, M. Botta, J. A. K. Howard, J. M. Moloney, M. Navet, D. Parker, M. Port and O. Rousseaux, *J. Am. Chem. Soc.*, 2000, **122**, 9781-9792.
15. S. Aime, A. Barge, M. Botta, D. Parker and A. S. DeSousa, *J. Am. Chem. Soc.*, 1997, **119**, 4767-4768.

16. R. S. Ranganathan, R. K. Pillai, N. Raju, H. Fan, H. Nguyen, M. F. Tweedle, J. F. Desreux and V. Jacques, *Inorg. Chem.*, 2002, **41**, 6846-6855.
17. P. H. Keizers, J. F. Desreux, M. Overhand and M. Ubbink, *J. Am. Chem. Soc.*, 2007, **129**, 9292-9293.
18. M. D. Vlasie, C. Comuzzi, A. M. C. H. van den Nieuwendijk, M. Prudencio, M. Overhand and M. Ubbink, *Chemistry-a European Journal*, 2007, **13**, 1715-1723.
19. M. A. Hass and M. Ubbink, *Curr Opin Struct Biol*, 2014, **24**, 45-53.
20. C. T. Loh, K. Ozawa, K. L. Tuck, N. Barlow, T. Huber, G. Otting and B. Graham, *Bioconjugate Chem.*, 2013, **24**, 260-268.
21. C. T. Loh, B. Graham, E. H. Abdelkader, K. L. Tuck and G. Otting, *Chemistry-a European Journal*, 2015, **21**, 5084-5092.
22. D. Haussinger, J. R. Huang and S. Grzesiek, *J. Am. Chem. Soc.*, 2009, **131**, 14761-14767.
23. S. Aime, M. Botta, M. Fasano, M. P. M. Marques, C. F. G. C. Geraldes, D. Pubanz and A. E. Merbach, *Inorg. Chem.*, 1997, **36**, 2059-2068.
24. S. Aime, M. Botta, M. Fasano, E. Terreno, P. Kinchesh, L. Calabi and L. Paleari, *Magnetic Resonance in Medicine*, 1996, **35**, 648-651.
25. R. S. Ranganathan, N. Raju, H. Fan, X. Zhang, M. F. Tweedle, J. F. Desreux and V. Jacques, *Inorg. Chem.*, 2002, **41**, 6856-6866.
26. S. Aime, M. Botta, Z. Garda, B. E. Kucera, G. Tircso, V. G. Young and M. Woods, *Inorg. Chem.*, 2011, **50**, 7955-7965.
27. M. Woods, Z. Kovacs, R. Kiraly, E. Brucher, Z. Sr and A. D. Sherry, *Inorg. Chem.*, 2004, **43**, 2845-2851.
28. M. P. M. Marques, C. F. G. C. Geraldes, A. D. Sherry, A. E. Merbach, H. Powell, D. Pubanz, S. Aime and M. Botta, *J. Alloys Compd.*, 1995, **225**, 303-307.
29. B. C. Webber and M. Woods, *Inorg. Chem.*, 2012, **51**, 8576-8582.
30. E. Csajbok, Z. Baranyai, I. Banyai, E. Brucher, R. Kiraly, A. Muller-Fahrnow, J. Platzek, B. Raduchel and M. Schafer, *Inorg. Chem.*, 2003, **42**, 2342-2349.
31. F. Benetollo, G. Bombieri, L. Calabi, S. Aime and M. Botta, *Inorg. Chem.*, 2003, **42**, 148-157.
32. A. C. Opina, K. J. Wong, G. L. Griffiths, B. I. Turkbey, M. Bernardo, T. Nakajima, H. Kobayashi, P. L. Choyke and O. Vasalatiy, *Nanomedicine (Lond)*, 2015, **10**, 1423-1437.
33. F. Delaglio, S. Grzesiek, G. W. Vuister, G. Zhu, J. Pfeifer and A. Bax, *J. Biomol. NMR*, 1995, **6**, 277-293.
34. A. Barge, G. Cravotto, E. Gianolio and F. Fedeli, *Contrast Media Mol Imaging*, 2006, **1**, 184-188.
35. G. A. Lazar, J. R. Desjarlais and T. M. Handel, *Protein Sci.*, 1997, **6**, 1167-1178.
36. W. F. Vranken, W. Boucher, T. J. Stevens, R. H. Fogh, A. Pajon, P. Llinas, E. L. Ulrich, J. L. Markley, J. Ionides and E. D. Laue, *Proteins-Structure Function and Bioinformatics*, 2005, **59**, 687-696.
37. Y. Zhao and D. G. Truhlar, *J. Chem. Phys.*, 2006, **125**, 194101-194118.
38. X. Y. Cao and M. Dolg, *J. Chem. Phys.*, 2001, **115**, 7348-7355.
39. M. J. T. Frisch, G. W.; Schlegel, H. B.; Scuseria, G. E.; Robb, M. A.; Cheeseman, J. R.; Scalmani, G.; Barone, V.; Mennucci, B.; Petersson, G. A.; Nakatsuji, H.; Caricato, M.; Li, X.; Hratchian, H. P.; Izmaylov, A. F.; Bloino, J.; Zheng, G.; Sonnenberg, J. L.; Hada, M.; Ehara, M.; Toyota, K.; Fukuda, R.; Hasegawa, J.; Ishida, M.; Nakajima, T.; Honda, Y.; Kitao, O.; Nakai, H.; Vreven, T.; Montgomery, J. A., Jr.; Peralta, J. E.; Ogliaro, F.; Bearpark, M.; Heyd, J. J.; Brothers, E.; Kudin, K. N.; Staroverov, V. N.; Kobayashi, R.; Normand, J.; Raghavachari, K.; Rendell, A.; Burant, J. C.; Iyengar, S. S.; Tomasi, J.; Cossi, M.; Rega, N.; Millam, J. M.; Klene, M.; Knox, J. E.; Cross, J. B.; Bakken, V.; Adamo, C.; Jaramillo, J.; Gomperts, R.; Stratmann, R. E.; Yazyev, O.; Austin, A. J.; Cammi, R.; Pomelli, C.; Ochterski, J. W.; Martin, R. L.; Morokuma, K.; Zakrzewski, V. G.; Voth, G.

A.; Salvador, P.; Dannenberg, J. J.; Dapprich, S.; Daniels, A. D.; Farkas, Ö.; Foresman, J. B.; Ortiz, J. V.; Cioslowski, J.; Fox, D. J., 2009.

RP-HPLC and NMR studies showed that early lanthanides of *SSSS*-*SSSS*-M4DOTMA unprecedentedly favor the SAP conformation, while late lanthanides adopt TSAP.